Macro Scale Material Characterization In Support Of Meso Scale Modelling Of Masonry Under Uniaxial In-Plane Loading

Anastasios Drougkas (corresponding) anastasios.drougkas@kuleuven.be

Leidy Bejarano-Urrego leidyelvira.bejaranourrego@kuleuven.be

Nathalie Van Roy nathalie.vanroy@kuleuven.be

Els Verstrynge els.verstrynge@kuleuven.be

Building Materials and Building Technology Division, Civil Engineering Department, KU Leuven, Kasteelpark Arenberg 40 Box 2448, B-3001 Heverlee, Belgium

Abstract

The amount of detailed experimental data on the mechanical properties of brick masonry available in the literature is limited as regards the orthotropic compression behaviour. These properties include both the strength and the fracture energy. This paper attempts to determine the mechanical properties of the masonry composite as a function of the properties of its components.

In this paper a combined experimental/numerical methodology is proposed for the derivation of the macro scale properties of masonry. The experimental aspect deals with the mechanical characterization of the individual materials, small masonry samples and, finally, masonry wallettes and includes the relation of couplet to wallette compressive strength. The numerical aspect is the calculation of the macroscopic properties of the masonry composite through calculations using discrete cracking models of the wallettes. Unknown material properties are taken from the available literature. The calculations are performed in two orthogonal in-plane directions. For evaluation, material properties for the meso-models are taken from laboratory testing and from the literature. The results of the numerical analyses are compared with the experimental stress-strain results and Digital Image Correlation (DIC) analysis. Parameters such as the Young's modulus and compressive fracture energy for the masonry composite are able to be derived. The results are analysed in view of the resulting anisotropy of masonry and the obtained failure modes.

This paper is a revised and expanded version of a paper entitled "Mechanical characterization of masonry on the macro scale from experimental testing and numerical meso scale modelling" presented at the 10th International Masonry Conference, Milan, Italy, 9-11 July 2018.

Keywords

Numerical analysis, masonry, discrete cracking, meso-modelling, macro-modelling

1. Introduction

1.1 State of the art

The derivation of the macroscopic mechanical properties of masonry composites from experimental and numerical testing is a complicated matter (Sarhosis, 2016). This derivation requires one of two approaches to be adopted: either testing of entire masonry samples or testing of small material samples, i.e. units, mortar and couplets, and subsequent upscaling. The first approach requires the construction of large samples, i.e. masonry prisms or wallettes (Adam, Brencich, Hughes, & Jefferson, 2010), which can be time-consuming and costly. Additionally, either of these approaches may require sample extraction (Pelà, Canella, Aprile, & Roca, 2016) in the case of existing structures where the material properties cannot be easily or reliably determined through non-destructive testing. As such the second approach is far more appealing and straightforward in execution. Substantial complexity arises from size effects influencing the mechanical testing, the compressive strength in particular (Drougkas, Roca, & Molins, 2016; Segura, Pelà, & Roca, 2018). This can affect both the units, from which it is difficult to extract compression samples with proper dimension ratios, and mortars, which may have different properties in stand-alone samples and in the joint. Further complexity is introduced by the well-documented variability of masonry materials, particularly in the case of existing and historic structures (Laefer, Boggs, & Cooper, 2008). This second approach is further associated with the additional step of calculating the macroscopic properties of the masonry composite from the individual properties of the component materials, which is not an easy task.

The construction and testing of masonry couplets and triplets requires far fewer resources and time than that of wallettes. Couplets are particularly advantageous for the investigation of existing and historic masonry structures due to the requirement of smaller amounts of original material. Extraction of masonry samples for

compressive testing is well documented in the literature, both for composites using lime (Pelà, Kasioumi, & Roca, 2017; Pelà, Roca, & Benedetti, 2016) and cement mortar (Brencich & Sterpi, 2006) and further proposed by recommendations for the assessment of existing masonry structures (International Union of Railways, 2011). However, a clear relation between the compressive strength of couplets and wallettes has not been established, despite related work with large 4- or 5-unit prisms (Gumaste, Nanjunda Rao, Reddy, & Jagadish, 2007; Vermeltfoort, Martens, & van Zijl, 2007). Given the large percentage of brick masonry structures built in running bond or similar variants, it is essential to establish a relation for the compressive strength of the two typologies.

A valuable tool during the execution of mechanical tests on masonry materials and members is digital image correlation (DIC). Through the use of a single digital camera monitoring a prepared surface of the sample, it is possible to obtain the full-field displacements of the sample. Strain maps can be subsequently created and related to the applied stresses at any given moment for the determination of the Young's modulus and the Poisson's ratio. Since no physical contact and no attached instruments are required for the application, DIC can be applied to samples of small size, on which the attachment of physical measurement devices is difficult or impossible. This technique has been applied to both masonry materials (Drdácký, Masin, Mekonone, & Slizkova, 2008) and entire members (Bejarano-Urrego, Verstrynge, Giardina, & Van Balen, 2018; Thamboo, Dhanasekar, & Yan, 2013). The use of DIC on masonry at the member scale has been generally used for the tracking of the formation of cracks and the evaluation of their width under increasing load, at which point the deformations are mostly concentrated at the failure lines and of a significant magnitude (Cotič, Jagličić, & Bosiljkov, 2014; Nghiem, Al Heib, & Emeriault, 2015; Ramos et al., 2015). A promising application of the method is for the evaluation of the elastic properties of the masonry composite in the elastic range under low loads and low strain magnitude.

For the numerical modelling of masonry structures different approaches may be adopted, distinguished by the level of detail. A unified terminology for the different approaches has not yet been established, necessitating the definition of the terminology followed in this paper. Micro-modelling requires the individual simulation of the units, the mortar and the unit-mortar interface. This approach additionally demands that the models account for the three-dimensional confinement of mortar in compression in order for the compressive strength of the composite to be correctly estimated (Drougkas, Roca, & Molins, 2019; Petracca et al., 2017; Sandoval & Arnau, 2017). In meso-modelling the behaviour of the interfaces in tension, compression and shear is lumped in nonlinear

interfaces between the units, which may themselves be linear elastic, nonlinear elastic or featuring potential cracks through the introduction of nonlinear interfaces in their area (Lourenço & Rots, 1997). Finally, macro-models treat the entire masonry as a homogenous nonlinear elastic continuum which may feature orthotropic behaviour (Pelà, Cervera, & Roca, 2013). This approach requires the experimental determination of the orthotropic properties of masonry since it cannot directly account for the geometric interlocking of the units and the orthotropy that it induces in the composite. Concerning the choice between methods, Noort (Noort, 2012) has recommended the use of meso-models rather than micro-models since the micro-models were found to be numerically unstable. Micro-models are also associated with significantly increased computational cost and model preparation time and effort. However, the main drawback of the meso-models, shared with micro-models but absent in macro-models, is the necessity for an approximation of the non-linear behaviour of the joint interface. While having been used for the study of walls under combined compression and in-plane shear, meso-models have not been employed for the evaluation of the orthotropic properties of masonry composites in compression.

1.2 Objectives

This paper proposes a meso-modelling based methodology to determine the orthotropic material properties of masonry composites using the isotropic properties of their components. The methodology initiates with a laboratory testing campaign to determine the mechanical properties of the masonry components. The methodology comprises of compression and bending tests on brick and mortar samples, as well as vertical compression tests on masonry couplets. Moreover, it includes compression tests on masonry panels, with about 43 cm side length, loaded vertically and horizontally (in a direction perpendicular and parallel to the bed joints respectively). The tests on the panels are monitored with Linear Variable Differential Transformers (LVDTs) as well as DIC which monitors and calculates the horizontal and vertical full-field displacement contour maps during the whole test. The DIC displacement fields are used for the determination of the orthotropic elastic properties of the masonry composite.

The next step includes the development of non-linear discrete cracking meso-models of the masonry panels subjected to compression in both orthogonal loading directions. The material characterization for the models is based on the laboratory testing campaign results and relevant literature. From these models, the stress-strain curves

for compression are determined and thus the masonry composite properties are obtained. These properties include the Young's Modulus E_m, compressive strength $f_{c,m}$ and Poisson's ratio ν_m.

Meso-modelling of masonry allows the calculation of the mechanical properties of masonry composites based on the results of experimental tests on small material samples. Micro-modelling can serve the same purpose, but involves far greater computational cost and modelling complexity. This aspect was investigated by Noort (Noort, 2012), who introduced an initial methodology using several bond types and considering the properties of the brick, mortar as well as the brick-mortar interface, for which micro-models instead of meso-models were used. However, several issues were faced regarding the numerical instability of such micro-models together with a lack of sufficient experimental data. The current methodology therefore implements the meso-modelling approach as well as a laboratory testing campaign on different sample sizes.

2. Lab Testing Campaign

2.1 Overview and scope

To characterize the mechanical properties of the masonry, an experimental campaign was performed on small samples of the masonry constituents as well as masonry couplets. Tests on masonry panels were executed as well. Mortar and brick samples were tested under compression and bending, while couplets and masonry panels were tested under compression, the latter ones in two orthogonal in-plane directions. Numerical meso-models of masonry panels under pure compression were built considering the obtained experimental material properties. From these meso-models, smeared material properties are determined aimed at characterizing macro-models.

The testing of couplets serves as an intermediate step between the testing of individual material samples and the testing of masonry wallettes. The construction and testing of wallette samples presents substantial advantages compared to wallettes in terms of economy and time investment. Further, in the particular case of historic masonry, the construction of couplets requires a very limited amount of extracted material. It is therefore worthwhile to attempt the determination of the properties of masonry composites as input for meso-scale models from the testing of masonry couplets.

The masonry is composed of solid clay bricks with dimensions 188 × 42 × 88 mm^3 and hybrid lime-cement mortar composed of river sand 0/2 (68.0 %), Portland cement CEM I 52.5 (5.6 %), hydrated lime (11.4 %) and water (15.0 %).

2.2 Material characterization on small samples

The compressive strength f_c and Young's modulus E were derived from uniaxial compression tests on mortar and brick cubes as well as on couplets. Six mortar samples and eight brick samples with dimensions 40 × 40 × 40 mm^3 were tested (Figure 1a). The loading scheme consists in an initial cyclic sequence and a final monotonic sequence. The cyclic sequence consisted in 3 loading and unloading branches, reaching the 10%, 25% and 50% of the anticipated peak stress. All loads were applied in displacement control at a rate of 0.2 mm/min in order to accurately register the softening branch. Measurements were taken from four LVDTs which were fixed on the loading plates at each corner of the cubes. The brick cubes were produced through cutting using a circular saw and were tested without the use of a compensating layer between sample and load plate, a smooth loading surface being produced by the cutting process. This approach precludes the deformation of a compensating layer in the case where the LVDTs are placed on the load plates. While a standard for the testing of masonry units in compression is available (CEN, 2011), it prescribes the testing of entire units and the adjustment of the results using numerical factors based on dimension ratios. The production of cubic samples allows the partial alleviation of size effects, as well as allowing the execution of the compressive testing of both mortar and units on similarly shaped samples using the same setup.

Three masonry couplets arranged with two bricks bound with a 12 mm mortar bed joint were also tested in compression at the age of 28 days using a cyclic load setup. The load was applied in displacement control at a rate of 0.5 mm/min. Two LVDTs were fixed on the opposite long sides of the couplets, as shown in Figure 1b. A gypsum layer was applied at the load surfaces of the samples to ensure a plane loading surface. Finally, a Teflon sheet was subsequently added between the gypsum layer and the load plates in order to reduce friction between the load plates and the samples.

The characterization of the flexural strength of bricks and mortar was done using three-point bending tests on specimens with size 40 × 40 × 160 mm^3 following EN1015-11 (CEN, 2007), as shown in Figure 1c. Loading was applied in displacement control at a rate of 0.2 mm/min.

Figure 1 Experimental setup for small samples: a) compression test on cubes, b) compression test on couplets and c) three-point bending test on small beams (clay brick shown here). Colour figure available in online version.

Figure 2 shows the stress-strain curves from the compression tests on the different samples. The naming convention for the 8 unit samples consists in a numerical value indicating the parent brick unit (1 through 4) and a letter (A or B) indicating the two samples extracted from the unit. A similar convention is followed for the mortar samples, with a parent mortar prism, tested in bending, and the two resulting halves indicated by a number and a letter respectively. Table 1 presents the average values of the test results. The brick samples, despite being of moderate strength, are clearly stronger than the mortar in compression. The compressive behaviour of the couplets is closer to the mortar, indicating the lower strength of the masonry joints compared to the units, but also a moderate confinement effect. The Young's modulus of the samples was measured as the secant modulus of the final loading branch of the cyclic loading sequence. The very low scatter of the couplet compressive strength is noteworthy, particularly in comparison with the higher scatter obtained from the brick tests.

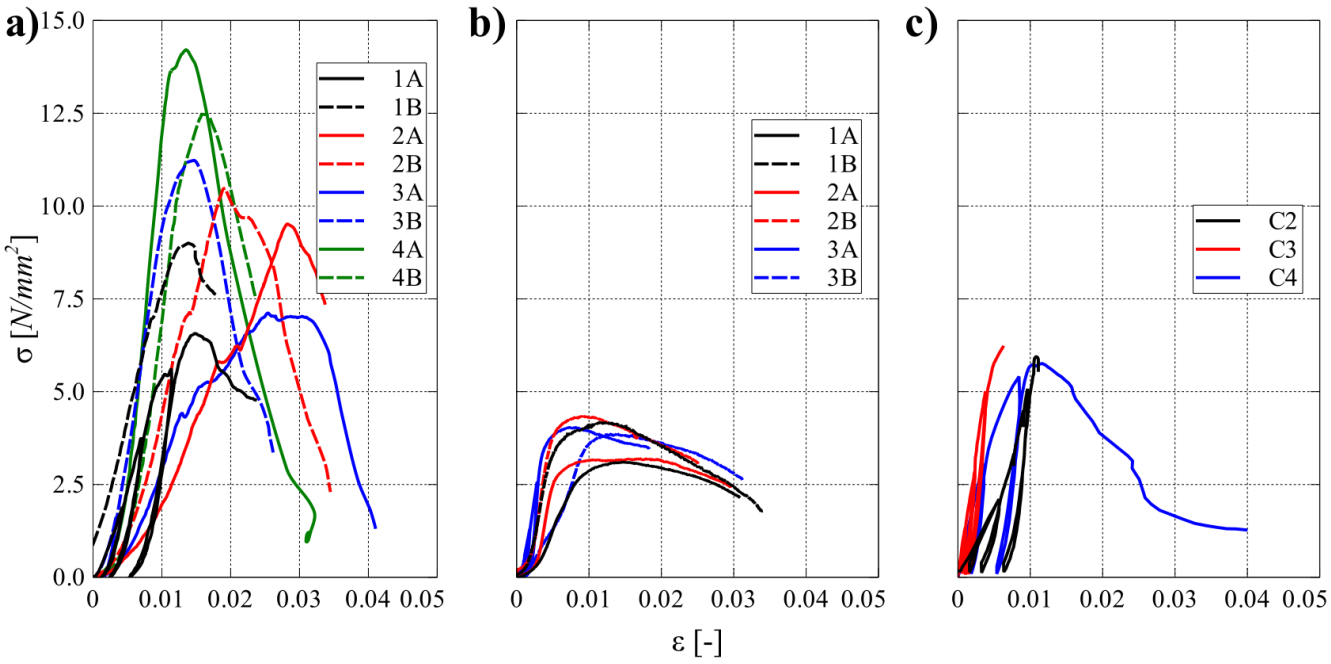

Figure 2 Stress-strain curves from compression tests: a) brick cubes, b) mortar cubes and c) couplets. Colour figure available in online version.

For couplet C4 it is possible to calculate the compressive fracture energy through integration of the area beneath the stress-displacement curve at the post-peak (Figure 2c). The choice of including only the post-peak part of the curve for this calculation is consistent with the compressive hardening/softening curve used in the combined cracking-shearing-crushing model employed in this paper (Lourenço & Rots, 1997), as well as the parabolic constitutive law proposed by Feenstra (Feenstra & Borst, 1996). This can be performed in a straightforward manner through trapezoidal integration of the data points according to the equation:

$$G_c = \sum_{n=2}^{N} H \cdot (\varepsilon(n) - \varepsilon(n-1)) \cdot \frac{\sigma(n-1) + \sigma(n)}{2} \quad (1)$$

where N is the total number of data points beyond the peak stress and H the total length of the sample along the direction of applied force. The high sampling rate allows for an accurate calculation using this numerical integration method. The equation yields a compressive fracture energy of 5.56 N/mm.

Table 1 Average mechanical properties obtained from tests on small samples.

Material	f_c [N/mm^2]	E [N/mm^2]	f_{flex} [N/mm^2]
Brick	9.62 (0.227)	2570 (0.297)	3.65 (0.066)
Mortar	3.00 (0.217)	920 (0.382)	0.92 (0.250)
Couplets	6.01 (0.035)	2025 (0.332)	-

Note: coefficient of variation indicated in parentheses

2.3 Tests on masonry panels

Additional compression tests were performed on four stretcher bond masonry panels, with 12 mm mortar joints, composed of 7 courses in height (426 mm), 2 brick units in width (391 mm) and 1 half brick in thickness (88 mm). Two masonry panels were loaded perpendicular to the bed joints, while the other two were loaded parallel to the bed joints, as shown in Figure 3. While a relevant standard was consulted for the construction and geometrical arrangement of the samples (CEN, 1999), the arrangement of the measurement setup was adapted according to the specific needs of this investigation and the placement of other sensors. Additionally, only two samples were tested in each direction as opposed to the suggested minimum of three.

Three vertical and one horizontal LVDTs were placed on one side of the panels to obtain displacements in both directions and to allow the calculation of the planar Poisson's ratio ν (Figure 3). On the other side of the panels, full-field vertical and horizontal displacements were monitored by means of stereo-vision digital image correlation (DIC) (Sutton, Orteu, & Schreier, 2009; Verstrynge et al., 2018). The application of DIC for the measurement of displacement fields on masonry structures under mechanical loading is a relatively novel but promising technique (Mojsilović & Salmanpour, 2016). The tests were executed using displacement control conditions at a loading rate of 0.5 mm/min. Both cyclic and monotonic compression tests were performed on the wallettes. Cyclic loads were applied up to about 10 kN, 20 kN, 30 kN and 40 kN of load, the final value corresponding to about 50% of the expected peak force.

The naming convention for the loading direction is based on the orientation of the masonry bond in actual structures. Therefore, vertical loading indicates an application of a load perpendicular to the bed joints and horizontal loading indicates an application of a load parallel to the bed joints.

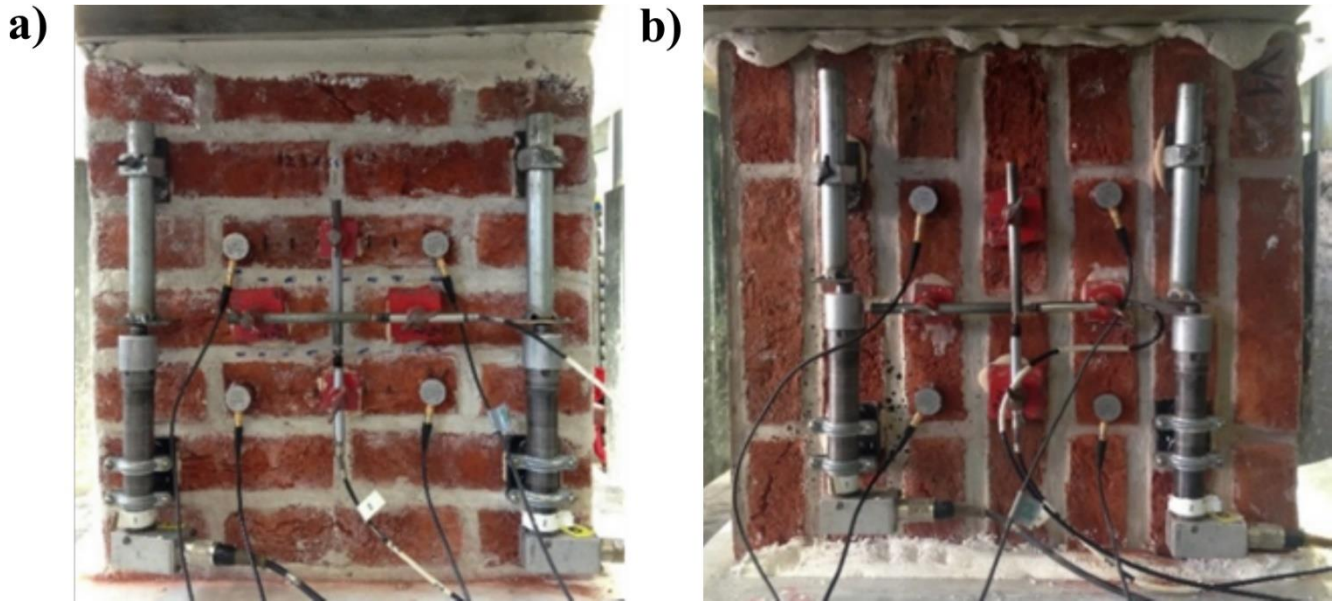

Figure 3 Setup of compression tests on masonry panels: a) perpendicular to the bed joints (vertical loading) and b) parallel to the bed joints (horizontal loading). Colour figure available in online version.

The initial cyclic tests are presented in Figure 4. Both the strains along the axis of loading and in the lateral direction are presented. The pairs of wallettes in either direction presented similar behaviour, as can be ascertained through comparison of the obtained curves. The higher stiffness of the wallettes in the horizontal direction is particularly apparent in the case of the H1 wallette, even for the low loads applied in the cycles. None of the wallettes presented visible cracking at the end of the cycles, nor was there any reduction in stiffness apparent in the obtained stress-strain curves.

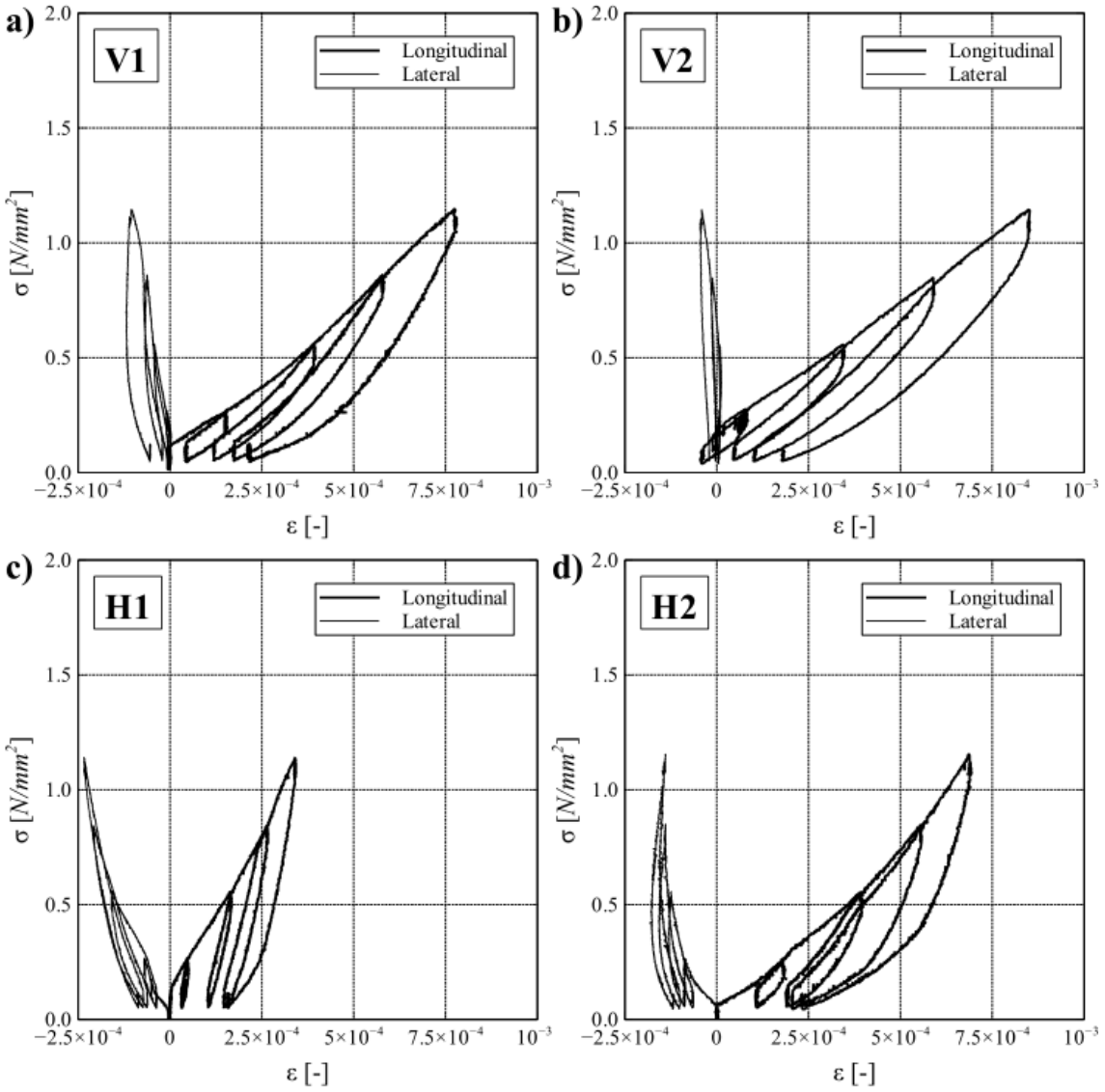

213

214 **Figure 4 Stress-strain graphs for wallettes in cyclic compression: a) V1, b) V2, c) H1 and d) H2**
215 **samples. V1 and V2 are wallettes subjected to vertical loading. H1 and H2 are wallettes subjected to**
216 **horizontal loading.**

217 The stress-strain curves as obtained in the subsequent monotonic compression tests for all the panels are
218 shown in Figure 5. The strains in both the longitudinal and lateral direction relative to the load application are
219 presented. They indicate a slightly higher stiffness on the panels loaded parallel to the bed joints (H1 and H2).
220 The compressive strength obtained was on average 2.66 N/mm^2, excepting one of the panels loaded vertically,
221 which only reached 1.85 N/mm^2. Table 2 shows the summary of the mechanical properties obtained from the tests
222 on the panels loaded in both directions. A small difference can be seen in the Poisson's ratio regarding the loading

direction. Due to a malfunction of the horizontal LVDT, the Poisson's ratio of the second wall tested horizontally (H2) was not correctly measured.

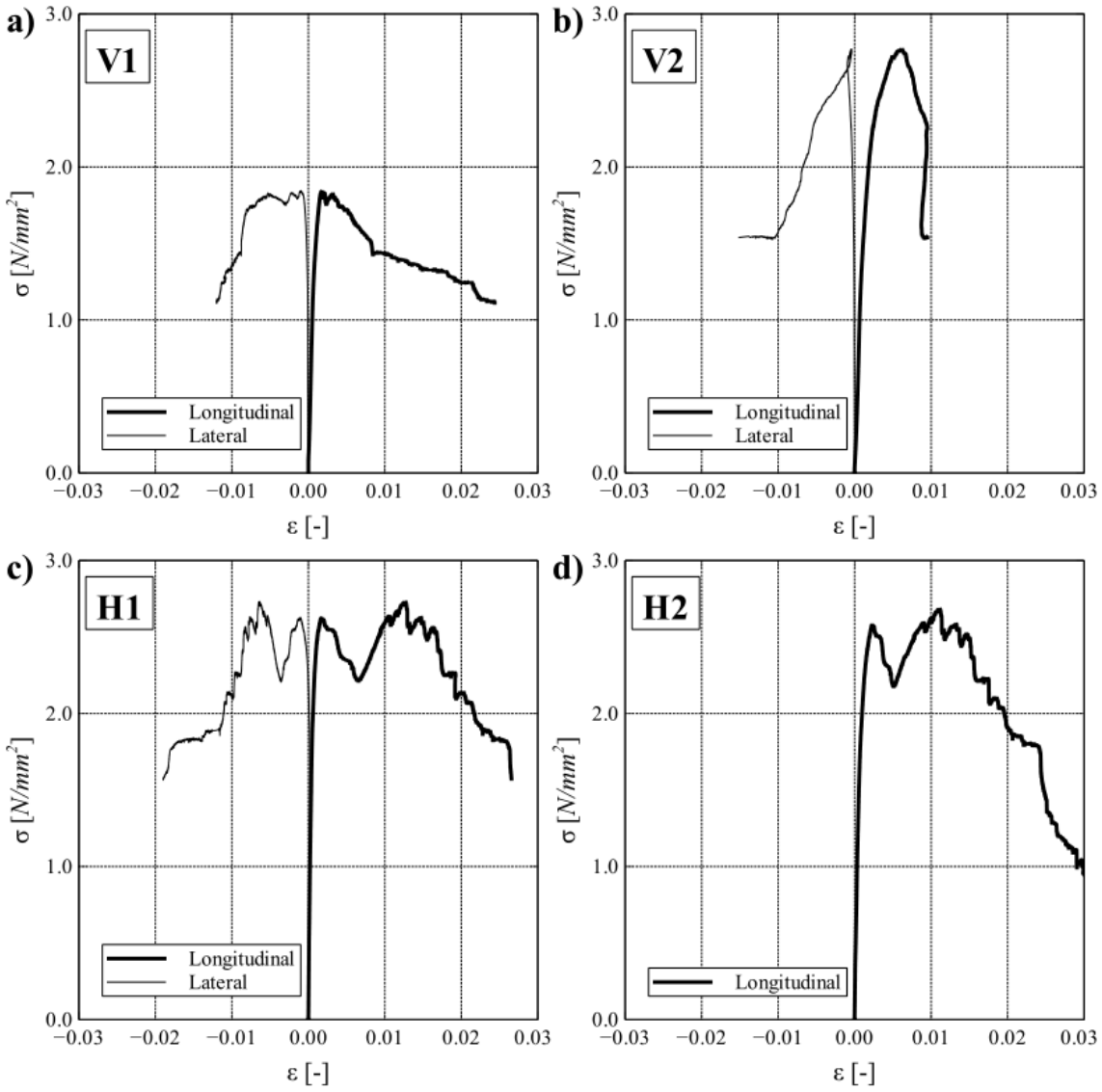

Figure 5 Stress-strain graphs for wallettes in monotonic compression: a) V1, b) V2, c) H1 and d) H2 samples.

It was found that the compressive strength values obtained from the panels are about half of the values obtained from the couplets (6.01 N/mm^2), but just slightly lower than the values from the mortar samples (3.00 N/mm^2). The Young's modulus was determined as the secant modulus of the final loading branch of the cyclic load sequence.

The compressive fracture energy as calculated by equation (2) yields values much higher than the value calculated for the couplets, which have a single mortar joint. This response can indicate either lateral confinement of the sample by the load plates, confinement of the mortar joint by the units, which can increase the apparent compressive fracture energy of the mortar, or a less localized crushing across several mortar joints, with possible contribution by the energy consumed in the failure of the units in compression and tension.

Table 2 Mechanical properties obtained from compression tests on masonry panels.

Panel	f_c [N/mm^2]	E [N/mm^2]	G_c [N/mm]	ν [N/mm^2]
V1	1.85	1776	22.13	0.18
V2	2.77	1453	4.47	0.14
Average vertical	*2.31*	*1615*	*13.30*	*0.16*
H1	2.63	3999	23.19	0.20
H2	2.59	2425	24.59	-
Average horizontal	*2.61*	*3212*	*23.89*	*0.20*
Average	***2.46***	***2610***	***18.60***	***0.17***

2.4 Discussion on results

The results obtained from the present experimental campaign are compared with results from the literature dealing with lime/cement mortars and solid clay units. The comparison of couplet and wallette test results, as well as of wallette tests in two orthogonal directions, is very uncommon in the literature. A number of instances are presented for comparison in Table 3. In terms of notation, f_{cu} and f_{cm} are the uniaxial compressive strength of the units and the mortar respectively, f_{cwv} and f_{cwh} are the compressive strength of wallettes in the vertical and horizontal direction and f_{cc} is the compressive strength of masonry couplets or triplets.

The compressive strength of the wallettes in the present case study appears to be atypical for lime/cement mortar masonry. The expected compressive strength normally lies between that of the units and the mortar in uniaxial compression (Drougkas, Verstrynge, Hayen, & Van Balen, 2019; Segura et al., 2018). The reason behind this low strength of the wallettes is not entirely clear, although it has been previously noted in experimental campaigns with low to moderate strength bricks coupled with moderate to high strength mortars (Binda, Fontana, & Frigerio, 1988; Gumaste et al., 2007; Kaushik, Rai, & Jain, 2007; Sarangapani, Reddy, & Jagadish, 2005). Nevertheless, similar ratios between the strength of couplets and wallettes were encountered in cases of lime/cement mortars (Verstrynge, Schueremans, & Van Gemert, 2011), with the couplets having a much higher strength than wallettes loaded vertically.

A substantial difference between the compressive strength of wallettes and couplets or triplets has been noted for the types of materials used in the present study and from available data in the literature (Drougkas, Roca, et al., 2019; Drougkas, Verstrynge, et al., 2019; Verstrynge et al., 2011). This can be attributed to size effects due to the dimension ratio difference between the samples, the existence of head joints in the wallettes and to less effective compaction of the bed joints during construction. Overall, the ratio of couplet or triplet strength to wallette vertical strength lies between 1.33 and 3.16 in the considered cases, including the present study.

A characteristically anisotropic response has been registered in the masonry wallettes. As in the present study, a slightly higher compressive strength in the horizontal direction over the vertical has been found in similar experimental campaigns (Drougkas, Roca, et al., 2019; Page, 1983). Assuming that the compaction of the mortar is equally well-performed in the head and the bed joints, the function of the bed joints in shear appears to be a factor influencing the response of the masonry wallettes in horizontal compression. The ratio of horizontal to vertical wallette compressive strength, both in the present case and in the literature, varies between 1.08 and 1.13. This agreement indicates that the average values of the compressive strength of the wallettes have been determined with some confidence despite the use of a limited number of samples.

Table 3 Comparison of present experimental findings with data from the literature.

Reference	f_{cu} $[N/mm^2]$	f_{cm} $[N/mm^2]$	f_{cwv} $[N/mm^2]$	f_{cwh} $[N/mm^2]$	f_{cc} $[N/mm^2]$	c/b $[-]$
Present study	9.62	3.00	2.31	2.61	6.01	0.33
(Segura et al., 2018)	17.93	1.91	6.51	-	-	-
(Drougkas, Verstrynge, et al., 2019)	9.97	1.70	4.70	-	8.12	0.61
(Verstrynge et al., 2011)	15.30	0.94	2.54	-	8.02	0.00
(Drougkas, Roca, et al., 2019)	35.00	8.34	15.20	16.90	20.20	1.00
(Page, 1983)	15.41	5.08	8.01	8.69	-	-

Close examination of the results from the literature and the present study reveals a clear relation between the cement content as a percentage of total binder c/b in the mortar and the ratio of couplet/triplet and vertical running bond wallette strength. The higher the cement content in the mortar the lower the compressive strength ratio. Given that lateral confinement of the joint mortar is of prime importance in the compressive strength of masonry, it follows that couplets and triplets provide much more effective confinement to the joints than running bond wallettes. The decrease of the strength ratio for higher cement content is consistent with the decrease in

importance, and in fact in the amount, of confinement for cement mortars with moderate to high compressive strength. The relation is illustrated in Figure 6, along with the least squares linear fit curve, which reads:

$$\frac{f_{cc}}{f_{cwv}} = -1.762(c/b) + 3.025 \tag{2}$$

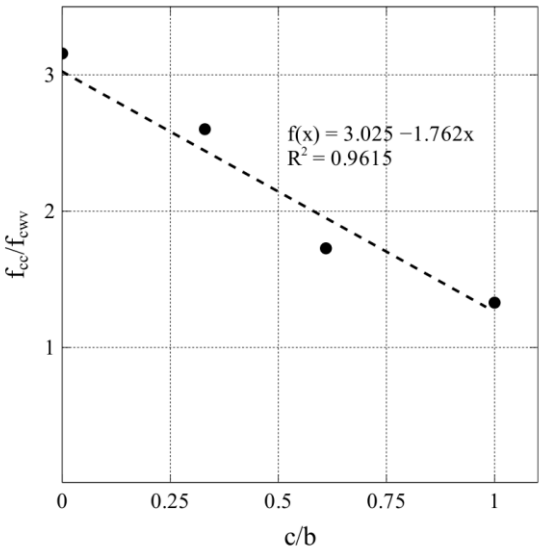

Figure 6 Relation between cement content in mortar binder and ratio of couplet/triplet to vertical wallette compressive strength.

3. Numerical analysis

Numerical analyses of the masonry panels using a meso-modelling approach were performed aiming to determine smeared parameters to characterize macro-models. This procedure was planned and implemented based on the work elaborated by Noort (Noort, 2012). The panel models were subjected to compression, as shown in Figure 7, allowing to obtain the stress-strain curves and parameters such as Young's Modulus E, compressive strength f_c and Poisson ratio ν.

3.1 Meso-modelling approach

The meso-modelling approach adopted is a discrete cracking model in which the damage is concentrated in relatively weak interfaces simulating the mortar joints by means of discrete non-linear interface elements with zero thickness. The brick elements are expanded to cover half of the width of the mortar joints and are represented by continuum linear elastic plane stress elements (Figure 7).

In this approach, masonry was modelled as a set of elastic elements bounded by potential fracture interfaces through the mortar joints. The meso-modelling strategy reduces geometrical complexity and computational costs compared to micro-modelling, in which bricks, mortar and the brick-mortar interfaces are modelled as different elements.

The non-linear behaviour of the joint interfaces was modelled using a combined cracking-shearing-crushing model proposed by Lourenço (Lourenço & Rots, 1997). The plasticity criterion includes three failure mechanisms: joint tensile cracking (Mode I), joint slipping (Mode II) and crushing (Mode III), in which softening behaviour takes place. The model is based on multi-surface plasticity and includes a Coulomb friction model combined with a tension cut-off and an elliptical compression cap (TNO, 2017). Therefore, all failure modes associated with masonry loaded in-plane are accounted for.

Brick units were represented by quadrilateral continuum plane stress elements with about 25 mm sides, with 8 nodes and 2 × 2 integration points, arranged as shown in Figure 7. Line interface elements with 6 nodes were adopted for the joints. The panel models were subjected to displacement uniformly applied on a very rigid plate attached at the side, from which the resulting reaction force was obtained. The opposite side of the panel was pinned.

The adopted material properties are listed in Table 4; they were chosen after a calibration procedure (Bejarano-Urrego et al., 2018) taking into account the experimental data from the tests on small samples and panels as well as data from literature (Drougkas, Roca, & Molins, 2015; Giardina, Hendriks, & Rots, 2015; Noort, 2012; Rots, 1997; Van der Pluijm, Rutten, & Ceelen, 2000). The interfaces are assigned the compressive strength of the wallettes in the vertical direction. In the general case, where it is intended to avoid tests on wallettes, the compressive strength determined from couplet testing may be modified according to equation (3) and used instead of the wallette strength. The normal stiffness $k_{n,i}$ and shear stiffness $k_{s,i}$ of the joint interfaces are estimated from the tests on the small samples by means of expressions (4), proposed by Lourenço (Lourenço & Rots, 1997), in terms of the Young's modulus of the brick E_b and mortar E_{mo}, the thickness of mortar layer t_{mo} and the Poisson's ratio. The cohesion of the joint interfaces c_i is assumed equal to 1.2 $f_{t,i}$ (Van der Pluijm et al., 2000). Three values were used for the compressive fracture energy: 5.56 N/mm as calculated from the couplet tests, 13.30 N/mm for

the wallettes in the vertical direction and 18.60 N/mm for the wallettes in the horizontal direction as calculated from the wallette compression experiments.

$$k_{n,i} = \frac{E_b E_{mo}}{t_{mo}(E_b - E_{mo})};\ k_{s,i} = \frac{G_b G_{mo}}{t_{mo}(G_b - G_{mo})};\ G_{b,mo} = \frac{E_{b,mo}}{2(1+\nu_{b,mo})} \quad (3)$$

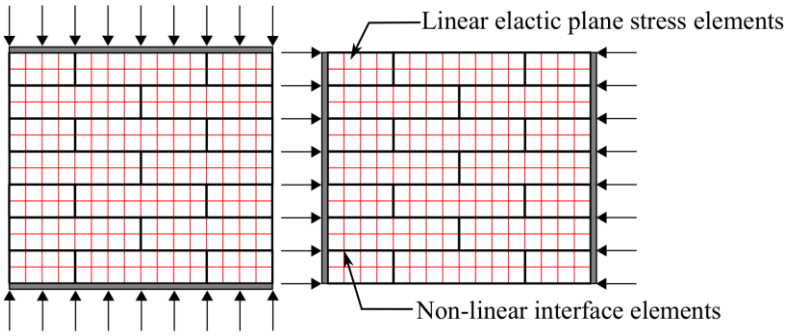

Figure 7 Meso-models of panels under compression. a) Load applied vertically (perpendicular to bed joints) and b) load applied horizontally (parallel to bed joints). Colour figure available in online version.

Table 4 Material parameters for the numerical model of the masonry panels

Material	Parameter	Symbol	Value	Units
Brick Units	Density	ρ_b	1875[a]	Kg/m^3
	Poisson's ratio	ν_b	0.2[c, b]	
	Young's modulus	E_b	2570[a]	N/mm^2
Joint Interfaces	Normal stiffness	$k_{n,i}$	119[a]	N/mm^3
	Shear stiffness	$k_{s,i}$	22[a]	N/mm^3
	Tensile strength	$f_{t,i}$	0.2[c]	N/mm^2
	Tensile fracture energy (Mode I)	$G_{t,i}$	0.012[c]	N/mm
	Cohesion	c_i	1.2 $f_{t,i}$ [c]	N/mm^2
	Friction angle	φ_i	36.9[c]	-
	Dilatancy angle	ψ_i	0	-
	Shear fracture energy (Mode II)	$G_{s,i}$	0.125[c]	N/mm
	Compressive strength	$f_{c,i}$	2.31[a]	N/mm^2
	Compressive fracture energy	$G_{c,i}$	5.56[a], 13.30[b], 18.6[b]	N/mm

Note: [a]: from tests on small samples, [b]: from tests on panels, [c]: from literature

3.2 Numerical analysis results

The experimental and numerical stress-strain curves of the panels loaded under compression are presented in Figure 8, indicating the loading direction: either horizontal (Hor.) or vertical (Ver.). Reasonable agreement is obtained between the experiments and the analyses. The masonry properties obtained from these meso-models,

for each loading direction, are the Young's modulus E_m, compressive strength $f_{c,m}$ and Poisson's ratio ν_m. All these smeared parameters are shown in Table 5.

The obtained peak force and failure mode depend on the direction of the loading. The failure mode is more straightforward in the vertical direction, with the response being dominated by the yielding of the bed joint in compression. The staggered arrangement of the head joints complicates the failure mode in the horizontal direction. This arrangement introduces shear stresses in the bed joints, whose resistance is overcome before sliding at the bed joint unit-mortar interface occurs. This contribution increases the obtained compressive strength in the horizontal direction.

In accordance with the experimental results, the model presented higher stiffness in compression when loaded horizontally, having a Young's modulus 1.3 times higher than in the other direction. However, this phenomenon is more marked in the experimental data, in which the Young's modulus of the masonry panels loaded vertically is about double. A similar phenomenon occurs with the Poisson's ratio, which is higher for loading horizontally due to higher transversal deformation (barrel-like distortion under compression). The compressive strength is similar for both models and in agreement with the experimental data.

The effect of the compressive fracture energy is also shown in Figure 8. Using the lower value calculated for the couplets results in a post-peak response not registered in the experimental tests. Using the higher value derived from the wallette compression tests yields a numerical result closer to the experimental stress-strain curves, particularly in the case of the horizontal compression.

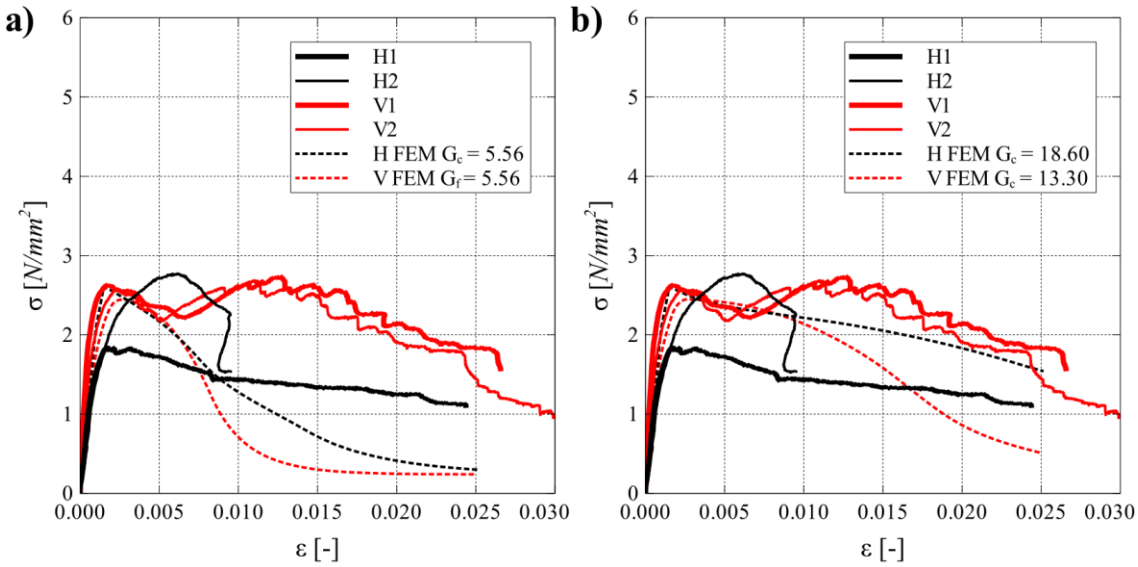

Figure 8 Comparison of stress-strain experimental and numerical results: a) wallettes with low compressive fracture energy and b) wallettes with high compressive fracture energy. Colour figure available in online version.

Table 5 Numerical analysis results from the masonry panel models.

Parameter	Symbol	Vertical	Horizontal	Units
Young's Modulus	E_m	1856	2291	N/mm^2
Poisson's ratio	ν_m	0.15	0.20	-
Compressive strength	$f_{c,m}$	2.31	2.60	N/mm^2

4. DIC results

Figure 9 shows the vertical displacement field at a level of applied force equal to 30 kN (0.87 N/mm^2) and 45 kN (1.31 N/mm^2) as monitored through DIC during the experiment. The coordinates are measured from the centre of the area of interest, or roughly the geometric centre of the wallette surface. Similarly, Figure 10 shows the vertical displacement field obtained from the meso-model for the same levels of applied load for a panel loaded under vertical compression. A speckle pattern coating was applied on the entire surface of the samples, constituting the area of interest for the measurements. This was despite the fact that masonry structures may not require the application of a speckle pattern, the measurements being capable of being acquired through the surface texture of the units and the mortar alone (Verstrynge et al., 2018). While the entire surface of the wallettes was considered in this analysis, it was necessary to exclude the results near the edges of the masonry wallettes. This

was due to the distortion they can cause in the presentation of the deformations. A buffer of 13 mm was thus employed, inwards from the edge of the samples.

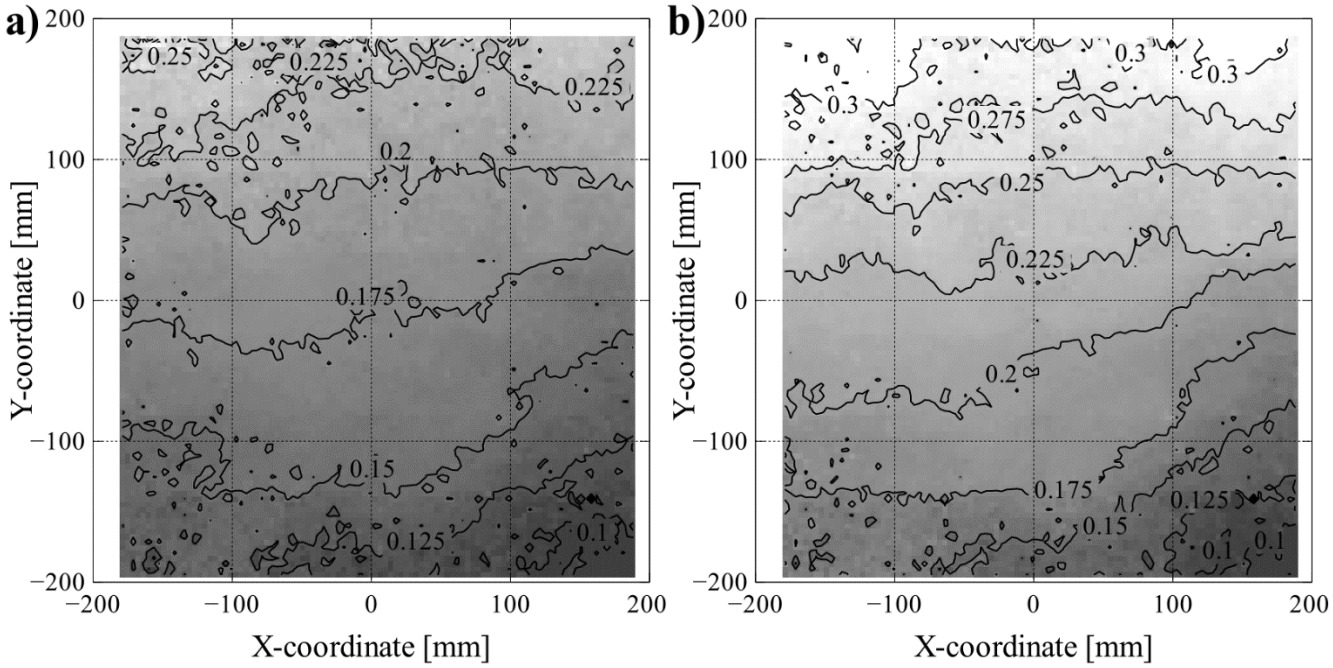

Figure 9 Experimental vertical displacement field in mm at a) 30 kN and b) 45 kN of applied load, monitored with the DIC technique for panel loaded under vertical compression (wallette V2).

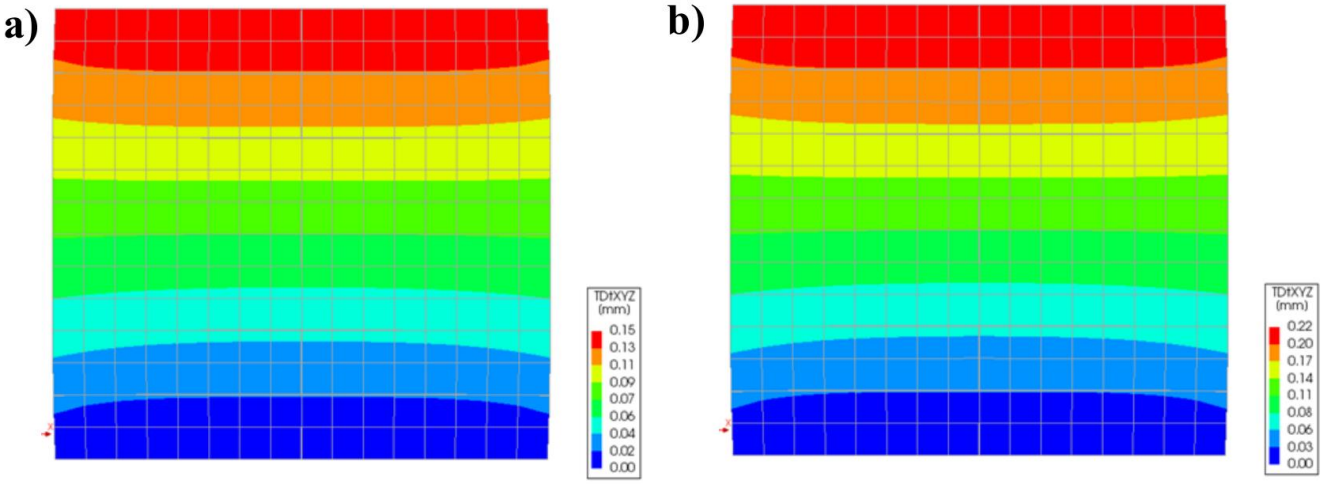

Figure 10 Numerically derived vertical displacement field in mm at a) 30 kN and b) 45 kN of applied load, obtained with the meso-model for panel loaded under vertical compression. Colour figure available in online version.

Following the processing of the DIC results, a vertical displacement of 0.175 mm is registered at the top of the sample for a load of 30 kN and 0.217 mm for a load of 45 kN. These values were obtained by determining the difference between the average deformation at the top of the measured surface and its base. The corresponding displacements obtained from the finite element meso-model analysis were 0.150 mm and 0.220 mm, meaning that an adequate degree of accuracy was achieved through the finite element models for in-plane compressive loading.

The Poisson's ratio of the wallettes was evaluated according to vertical and horizontal deformation data at the elastic range of the monotonic loading branch, both at the outer edges of the samples and at the inner third of their surface. The results are summarized in Table 6. The average values of the Poisson's ratio in the vertically loaded wallettes are equal for the outer and inner measurements. In the horizontal loading case, however, the outer measurements are affected by the lateral movement of the unrestrained outer header units, resulting in a higher apparent Poisson's ratio. The Poisson's ratio at the inner third is in relatively good agreement in comparison both with the LVDT results and the FE analysis.

Table 6 Poisson's ratio of wallettes derived from DIC data.

	Poisson's ratio	
Sample	Inner	Outer
V1	0.198	0.161
V2	0.137	0.174
Average vertical	0.168	0.168
H1	0.216	0.277
H2	0.223	0.785
Average horizontal	0.220	0.531

The DIC measurements further serve to highlight certain details of the response of the wallettes in compression. The displacement field in the finite elements analysis is purely symmetrical. In the experiment the vertical displacement field indicates slightly higher vertical deformation to the left of the sample. This can be attributed to imperfections of the sample itself, of the contact with the load plates or localized material weakness and failure.

Overall, it is demonstrated that DIC can be successfully employed in masonry member destructive tests not only for the tracking of crack widths but also for the determination of the elastic properties of the composite. The main practical advantage of this approach is the lack of need for the attachment of LVDTs or strain gauges. This

allows the evaluation of data after the formation of cracks that would cause detachment of physical gauges. The DIC measurements are accurate enough in the elastic range for the elastic properties to be successfully determined, despite the very small displacement magnitude and the surface irregularity of the samples.

5. Remarks and Conclusions

This work presents a methodology to determine composite masonry properties from numerical meso-models of masonry panels subjected to compression in two directions, parallel and perpendicular to the bed joints. The numerical analysis is performed using experimental data from small material samples: units, mortar and masonry couplets. An expression linking the compressive strength of couplets and wallettes in the vertical direction is proposed. The methodology eschews both complicated three-dimensional modelling required by micro-models and orthotropic experimental testing of wallettes.

The experimental data showed important anisotropy related to stiffness and Poisson's ratio presenting higher values for the panels loaded parallel to the bed joints. This phenomenon was noted in the meso-models, although slightly less pronounced.

The calculation of the compressive fracture energy of masonry wallettes from tests on couplets remains challenging. While a fair prediction of the compressive strength and the failure initiation mode may be obtained from couplet tests, the compressive fracture energy may differ significantly between the two setups. Numerical analysis using meso-models serves to highlight this fact, which also has a bearing on simulations using macro-models. Full three-dimensional analysis using micro-models may account for this discrepancy once computational costs can be reduced to acceptable levels.

The determination of all necessary material parameters for a meso-model from extracted samples is a challenging task. The paper demonstrates that the orthotropic properties of masonry in compression can be determined from a limited number of compression tests on small samples. Additional work is being carried out for the relation of the compressive strength of full-brick masonry couplets to small diameter cylindrical masonry couplets.

Since masonry is a very heterogeneous and anisotropic material, and its mechanical behaviour is influenced by several factors such as loading, type of components and bond type, future work will require an extensive lab testing campaign and related smeared macro-models to validate the presented methodology. In addition, the influence of different brick-mortar compositions will be investigated. Finally, further research will include validation of the methodology by means of smeared cracking models considering the parameters determined through, and the results of, experimental tests on larger masonry elements.

References

Adam, J. M., Brencich, A., Hughes, T. G., & Jefferson, T. (2010). Micromodelling of eccentrically loaded brickwork: Study of masonry wallettes. *Engineering Structures*, *32*(5), 1244–1251. https://doi.org/10.1016/j.engstruct.2009.12.050

Bejarano-Urrego, L.-E., Verstrynge, E., Giardina, G., & Van Balen, K. (2018). Crack growth in masonry: Numerical analysis and sensitivity study for discrete and smeared crack modelling. *Engineering Structures*, *165*(February), 471–485. https://doi.org/10.1016/j.engstruct.2018.03.030

Binda, L., Fontana, A., & Frigerio, G. (1988). Mechanical behaviour of brick masonries derived from unit and mortar characteristics. In *8th International Brick and Block Masonry Conference, Vol.1, Dublin, Ireland* (pp. 205–216).

Brencich, A., & Sterpi, E. (2006). Compressive Strength of Solid Clay Brick Masonry: Calibration of Experimental Tests and Theoretical Issues. In *Structural Analysis of Historical Constructions, New Delhi, India* (pp. 757–766).

CEN. (1999). *EN 1052-1 - Methods of test for masonry - Part 1: Determination of compressive strength*.

CEN. (2007). *EN 1015-11 - Methods of test for mortar for masonry - Part 11: Determination of flexural and compressive strength of hardened mortar*.

CEN. (2011). *EN 772-1 - Methods of test for masonry units. - Part 1: Determination of compressive strength*.

Cotič, P., Jagličić, Z., & Bosiljkov, V. (2014). Validation of non-destructive characterization of the structure and

seismic damage propagation of plaster and texture in multi-leaf stone masonry walls of cultural-artistic value. *Journal of Cultural Heritage*, *15*(5), 490–498. https://doi.org/10.1016/j.culher.2013.11.004

Drdácký, M., Masin, D., Mekonone, M. D., & Slizkova, Z. (2008). Compression tests on non-standard historic mortar specimens. In *1st Historical Mortar Conference, 24-26 September 2008, Lisbon* (pp. 24–26).

Drougkas, A., Roca, P., & Molins, C. (2015). Numerical prediction of the behavior, strength and elasticity of masonry in compression. *Engineering Structures*, *90*, 15–28. https://doi.org/10.1016/j.engstruct.2015.02.011

Drougkas, A., Roca, P., & Molins, C. (2016). Compressive strength and elasticity of pure lime mortar masonry. *Materials and Structures*, *49*(3), 983–999. https://doi.org/10.1617/s11527-015-0553-2

Drougkas, A., Roca, P., & Molins, C. (2019). Experimental Analysis and Detailed Micro-Modeling of Masonry Walls Subjected to In-Plane Shear. *Engineering Failure Analysis*, *95*, 82–95. https://doi.org/10.1016/j.engfailanal.2018.08.030

Drougkas, A., Verstrynge, E., Hayen, R., & Van Balen, K. (2019). The confinement of mortar in masonry under compression: Experimental data and micro-mechanical analysis. *International Journal of Solids and Structures*, *162*(May), 105–120. https://doi.org/10.1016/j.ijsolstr.2018.12.006

Feenstra, P. H., & Borst, R. De. (1996). A composite plasticity model for concrete. *International Journal of Solids and Structures*, *33*(5), 707–730.

Giardina, G., Hendriks, M., & Rots, J. G. (2015). Sensitivity study on tunnelling induced damage to a masonry façade. *Engineering Structures*, *89*, 111–129. https://doi.org/10.1016/j.engstruct.2015.01.042

Gumaste, K. S., Nanjunda Rao, K. S., Reddy, B. V. V., & Jagadish, K. S. (2007). Strength and elasticity of brick masonry prisms and wallettes under compression. *Materials and Structures*, *40*(2), 241–253. https://doi.org/10.1617/s11527-006-9141-9

International Union of Railways. (2011). *Leaflet 778-3R, Recommendations for the inspection, assessment and maintenance of masonry arch bridges*. Paris.

Kaushik, H. B., Rai, D. C., & Jain, S. K. (2007). Stress-Strain Characteristics of Clay Brick Masonry under Uniaxial Compression. *Journal of Materials in Civil Engineering*, (September), 728–739.

Laefer, D. F., Boggs, J., & Cooper, N. (2008). Engineering Properties of Historic Brick: Variability Considerations as a Function of Stationary versus Nonstationary Kiln Types. *Journal of the American Institute for Conservation*, *43*(3), 255. https://doi.org/10.2307/4129639

Lourenço, P., & Rots, J. G. (1997). Multisurface interface model for analysis of masonry structures. *Journal of Engineering Mechanics*, *123*(7), 660.

Mojsilović, N., & Salmanpour, A. H. (2016). Masonry walls subjected to in-plane cyclic loading: application of digital image correlation for deformation field measurement. *International Journal of Masonry Research and Innovation*, *1*(2), 165–187. https://doi.org/10.1504/IJMRI.2016.077473

Nghiem, H. L., Al Heib, M., & Emeriault, F. (2015). Method based on digital image correlation for damage assessment in masonry structures. *Engineering Structures*, *86*, 1–15. https://doi.org/10.1016/j.engstruct.2014.12.021

Noort, J. R. (2012). *Computational Modelling of Masonry Structures* (MSc dissertation). Delft.

Page, A. W. (1983). The strength of brick masonry under biaxial tension-compression. *International Journal of Masonry Construction*, *3*(1), 26–31.

Pelà, L., Canella, E., Aprile, A., & Roca, P. (2016). Compression test of masonry core samples extracted from existing brickwork. *Construction and Building Materials*, *119*, 230–240. https://doi.org/10.1016/j.conbuildmat.2016.05.057

Pelà, L., Cervera, M., & Roca, P. (2013). An orthotropic damage model for the analysis of masonry structures. *Construction and Building Materials*, *41*, 957–967. https://doi.org/10.1016/j.conbuildmat.2012.07.014

Pelà, L., Kasioumi, K., & Roca, P. (2017). Experimental evaluation of the shear strength of aerial lime mortar brickwork by standard tests on triplets and non-standard tests on core samples. *Engineering Structures*, *136*, 441–453. https://doi.org/10.1016/j.engstruct.2017.01.028

Pelà, L., Roca, P., & Benedetti, A. (2016). Mechanical Characterization of Historical Masonry by Core Drilling and Testing of Cylindrical Samples. *International Journal of Architectural Heritage*, *10*(2–3), 360–374. https://doi.org/10.1080/15583058.2015.1077906

Petracca, M., Pelà, L., Rossi, R., Zaghi, S., Camata, G., & Spacone, E. (2017). Micro-scale continuous and discrete numerical models for nonlinear analysis of masonry shear walls. *Construction and Building Materials*, *149*, 296–314. https://doi.org/10.1016/j.conbuildmat.2017.05.130

Ramos, T., Furtado, A., Eslami, S., Alves, S., Rodrigues, H., Arêde, A., … Moreira, P. M. G. P. (2015). 2D and 3D Digital Image Correlation in Civil Engineering - Measurements in a Masonry Wall. *Procedia Engineering*, *114*, 215–222. https://doi.org/10.1016/j.proeng.2015.08.061

Rots, J. G. (1997). *Structural masonry: An experimental/numerical basis for practical design rules*. Report 171, CUR, Gouda, The Netherlands.

Sandoval, C., & Arnau, O. (2017). Experimental characterization and detailed micro-modeling of multi-perforated clay brick masonry structural response. *Materials and Structures/Materiaux et Constructions*, *50*(1). https://doi.org/10.1617/s11527-016-0888-3

Sarangapani, G., Reddy, B. V. V., & Jagadish, K. S. (2005). Brick-Mortar Bond and Masonry Compressive Strength. *Journal of Materials in Civil Engineering*, (April), 229–237.

Sarhosis, V. (2016). Optimisation procedure for material parameter identification for masonry constitutive models. *International Journal of Masonry Research and Innovation*, *1*(1), 48–58.

Segura, J., Pelà, L., & Roca, P. (2018). Monotonic and cyclic testing of clay brick and lime mortar masonry in compression. *Construction and Building Materials*, *193*, 453–466. https://doi.org/10.1016/j.conbuildmat.2018.10.198

Sutton, M. A., Orteu, J. J., & Schreier, H. (2009). *Image Correlation for Shape, Motion and Deformation Measurements: Basic Concepts,Theory and Applications*. Springer US.

Thamboo, J. A., Dhanasekar, M., & Yan, C. (2013). Flexural and shear bond characteristics of thin layer polymer

cement mortared concrete masonry. *Construction and Building Materials*, *46*, 104–113. https://doi.org/10.1016/j.conbuildmat.2013.04.002

TNO. (2017). DIANA Finite Element Analysis, User's Manual. (J. Manie & W. P. Kikstra, Eds.). Delft: TNO DIANA BV.

Van der Pluijm, R., Rutten, H., & Ceelen, M. (2000). Shear behavior of bed joints. In *12th International Brick/Block Masonry Conference* (pp. 1849–1862).

Vermeltfoort, A., Martens, D. R. W., & van Zijl, G. (2007). Brick–mortar interface effects on masonry under compression. *Canadian Journal of Civil Engineering*, *34*(11), 1475–1485. https://doi.org/10.1139/L07-067

Verstrynge, E., Schueremans, L., & Van Gemert, D. (2011). Time-dependent mechanical behavior of lime-mortar masonry. *Materials and Structures*, *44*(1), 29–42. https://doi.org/10.1617/s11527-010-9606-8

Verstrynge, E., Wilder, K. De, Drougkas, A., Voet, E., Van Balen, K., & Wevers, M. (2018). Crack monitoring in historical masonry with distributed strain and acoustic emission sensing techniques. *Construction and Building Materials*, *162*, 898–907. https://doi.org/10.1016/j.conbuildmat.2018.01.103

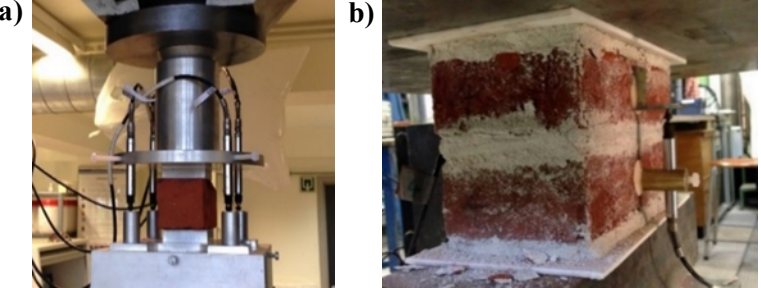
a)
b)
c)

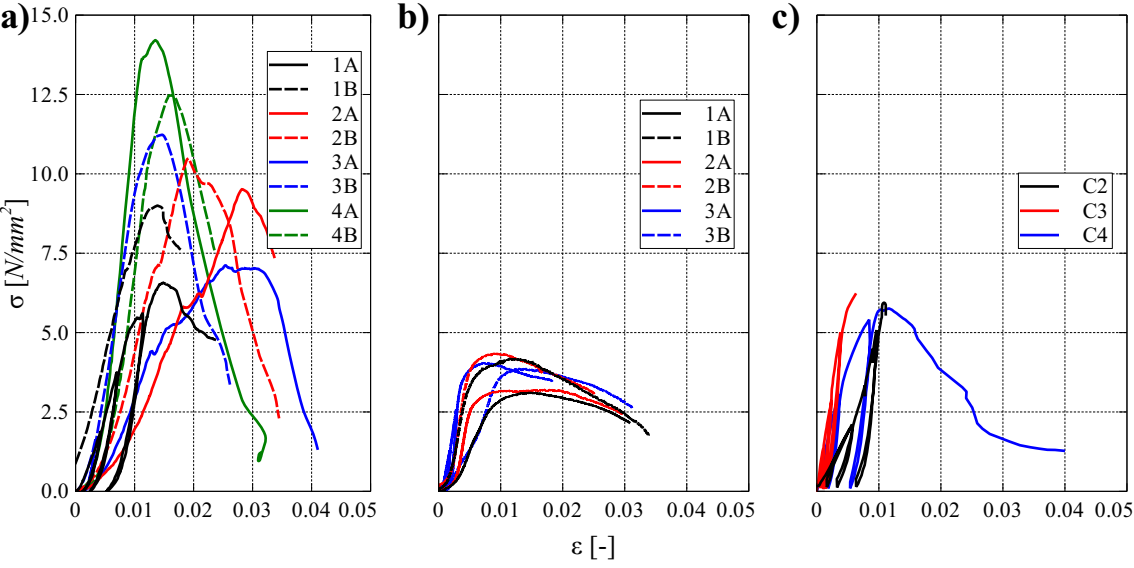
a)
b)
c)
σ [N/mm²]
ε [-]
1A
1B
2A
2B
3A
3B
4A
4B
C2
C3
C4
0.0
2.5
5.0
7.5
10.0
12.5
15.0
0
0.01
0.02
0.03
0.04
0.05

a)

b)

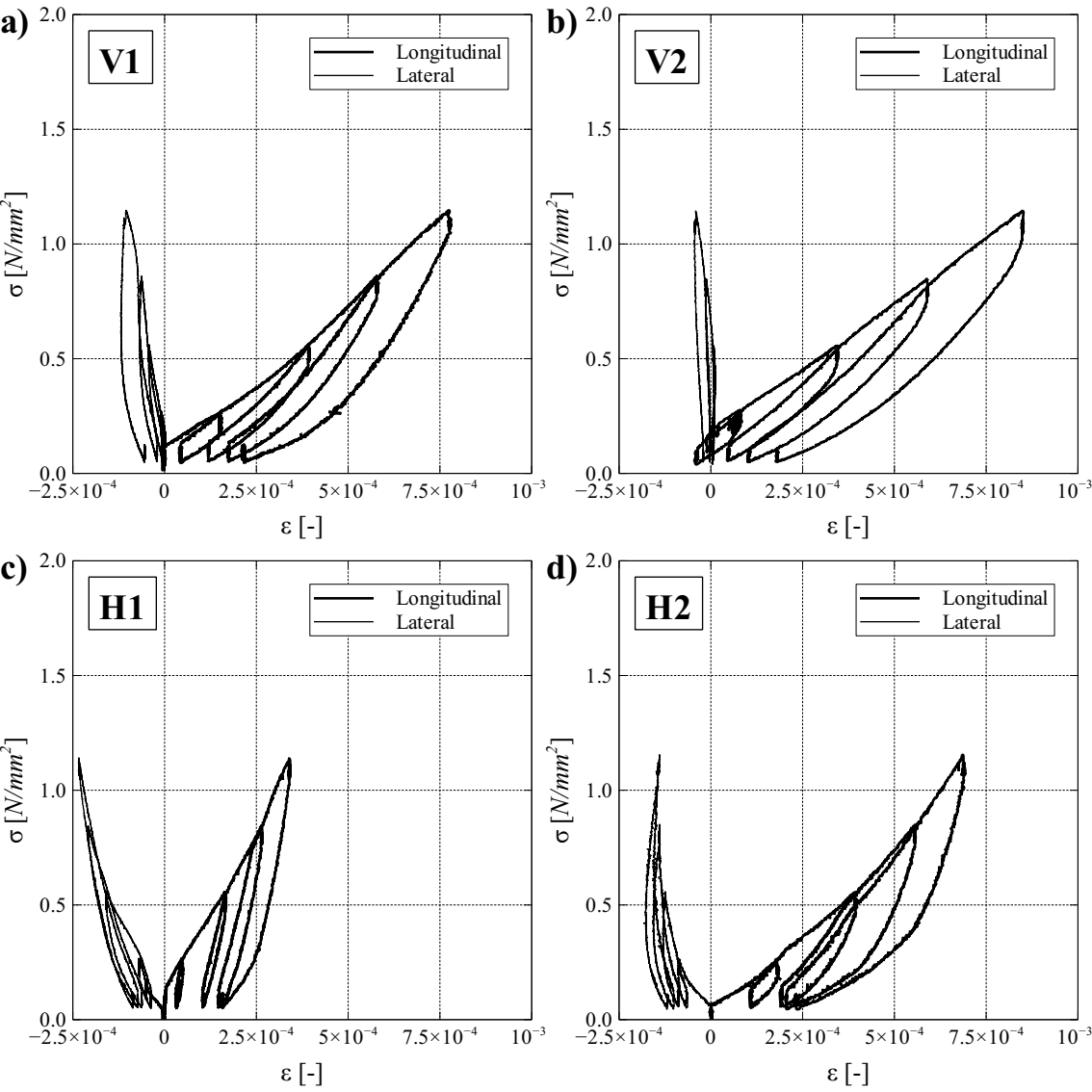
a)
V1
Longitudinal
Lateral
σ [N/mm²]
ε [-]
b)
V2
Longitudinal
Lateral
σ [N/mm²]
ε [-]
c)
H1
Longitudinal
Lateral
σ [N/mm²]
ε [-]
d)
H2
Longitudinal
Lateral
σ [N/mm²]
ε [-]
0.0
0.5
1.0
1.5
2.0
−2.5×10⁻⁴
0
2.5×10⁻⁴
5×10⁻⁴
7.5×10⁻⁴
10⁻³

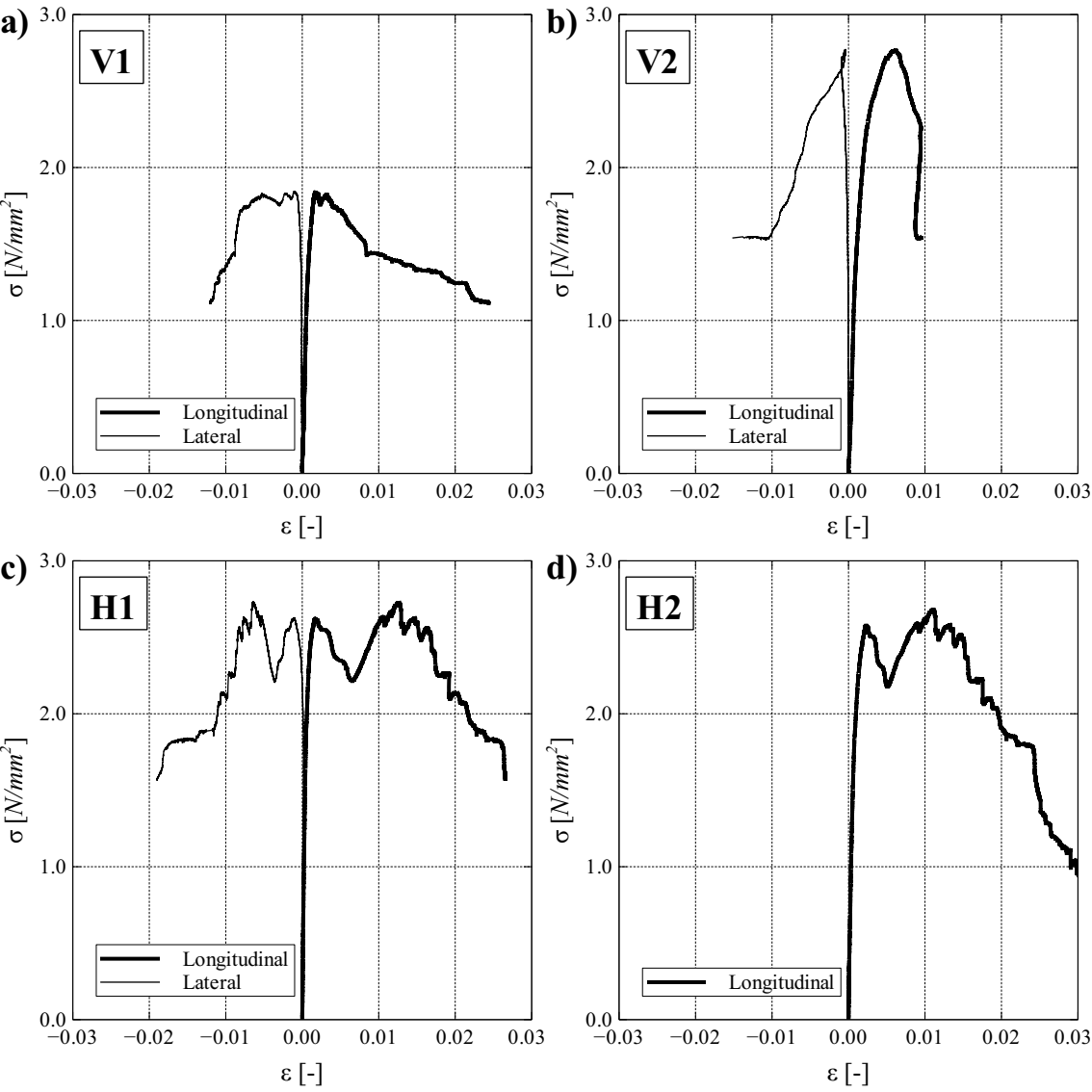
a)
V1
b)
V2
c)
H1
d)
H2
σ [N/mm²]
ε [-]
Longitudinal
Lateral
3.0
2.0
1.0
0.0
−0.03
−0.02
−0.01
0.00
0.01
0.02
0.03

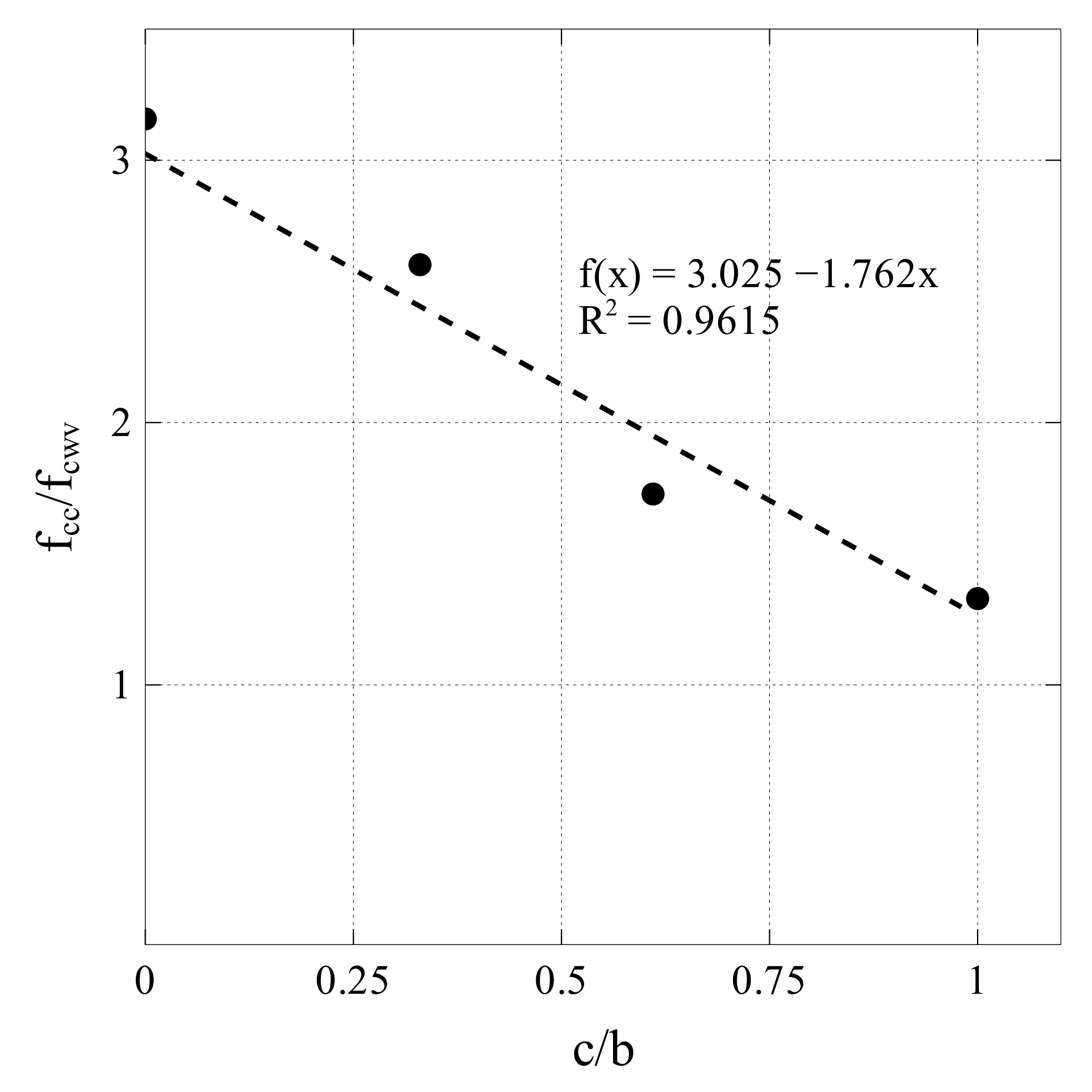
f(x) = 3.025 −1.762x
R2 = 0.9615
fcc/fcwv
c/b
0
0.25
0.5
0.75
1
1
2
3

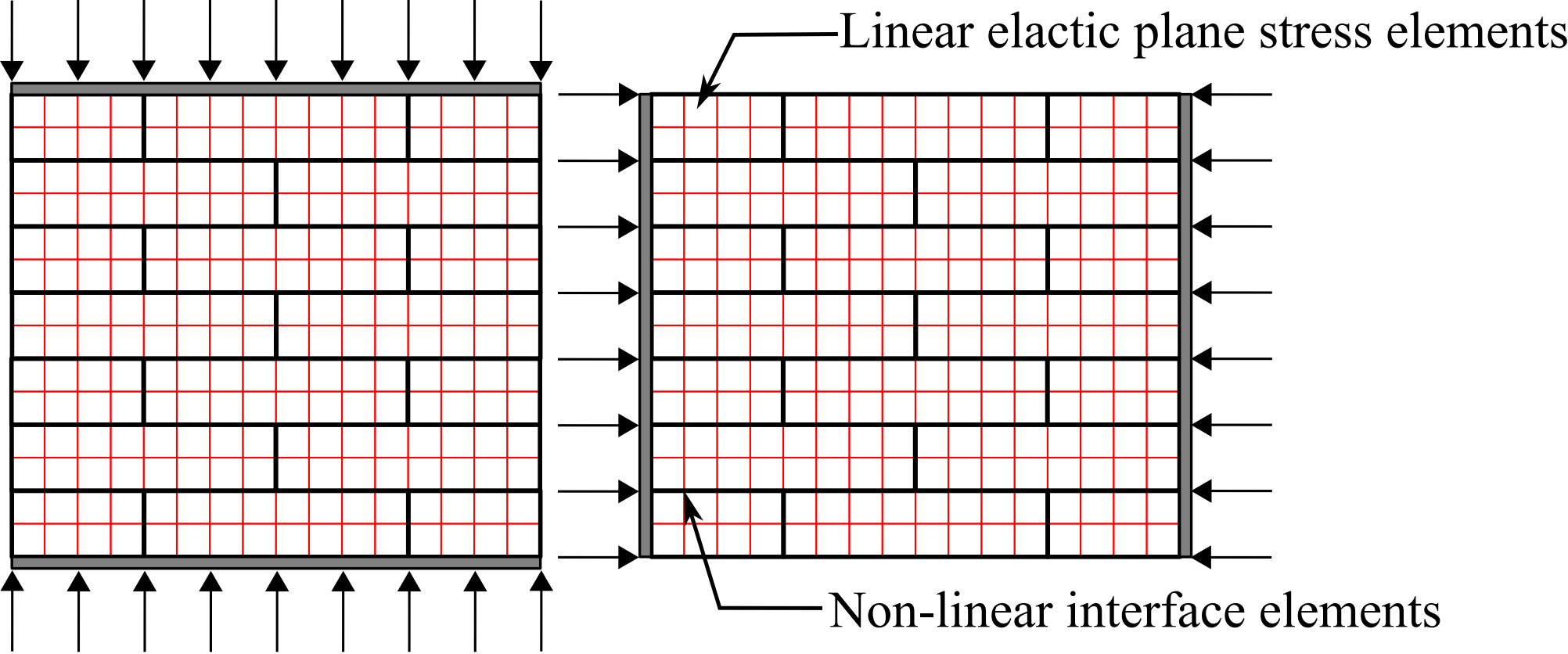
Linear elactic plane stress elements
Non-linear interface elements
a)
b)

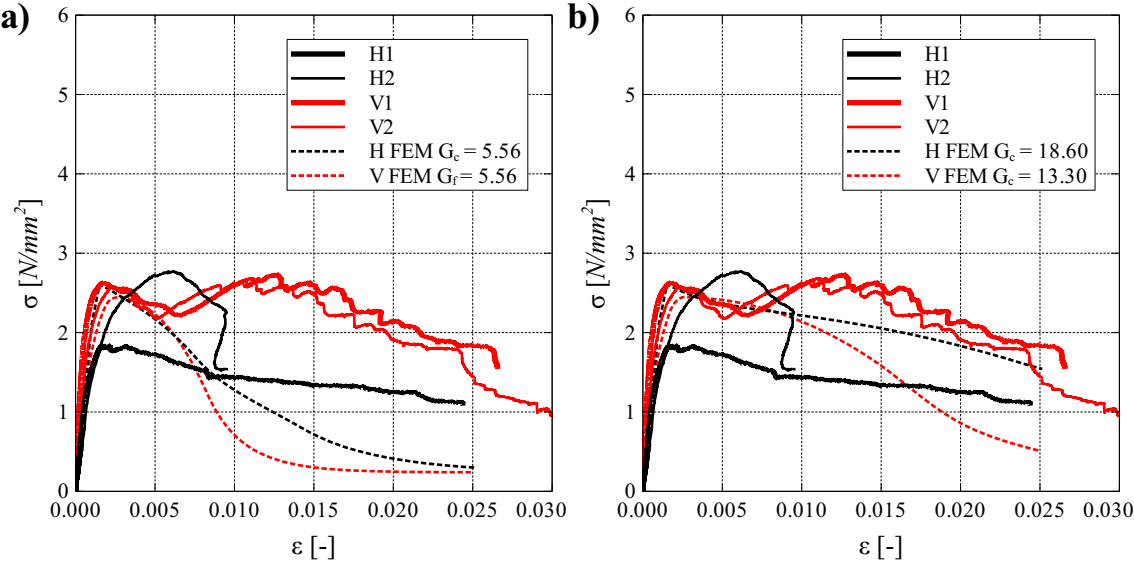
a)
b)
H1
H2
V1
V2
H FEM G_c = 5.56
V FEM G_f = 5.56
H FEM G_c = 18.60
V FEM G_c = 13.30
σ [N/mm^2]
ε [-]
0
1
2
3
4
5
6
0.000
0.005
0.010
0.015
0.020
0.025
0.030

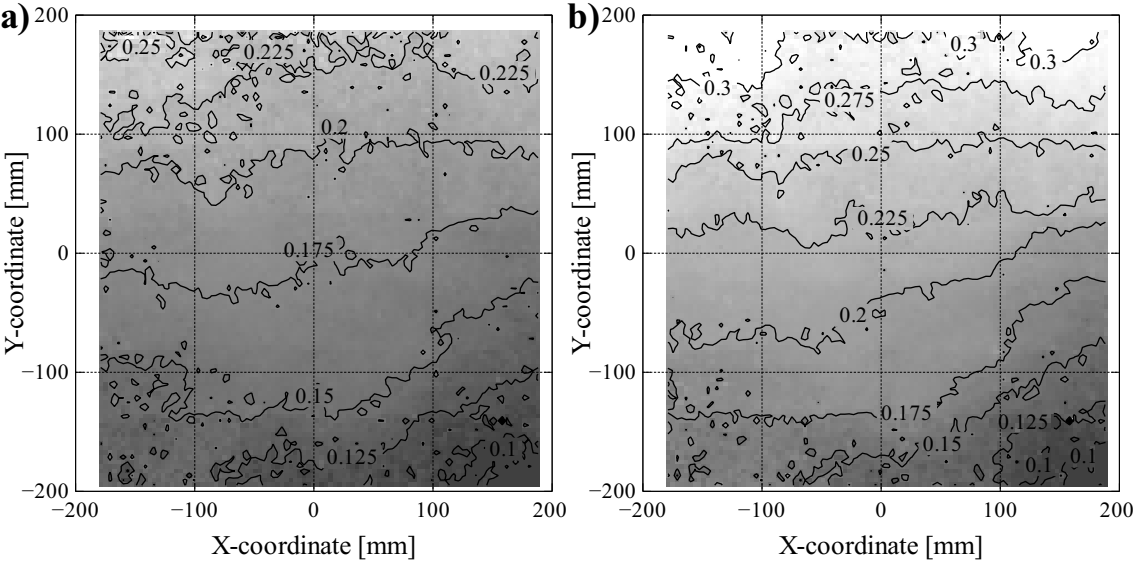
a)
b)
Y-coordinate [mm]
X-coordinate [mm]
200
100
0
−100
−200
0.25
0.225
0.2
0.175
0.15
0.125
0.1
0.3
0.275

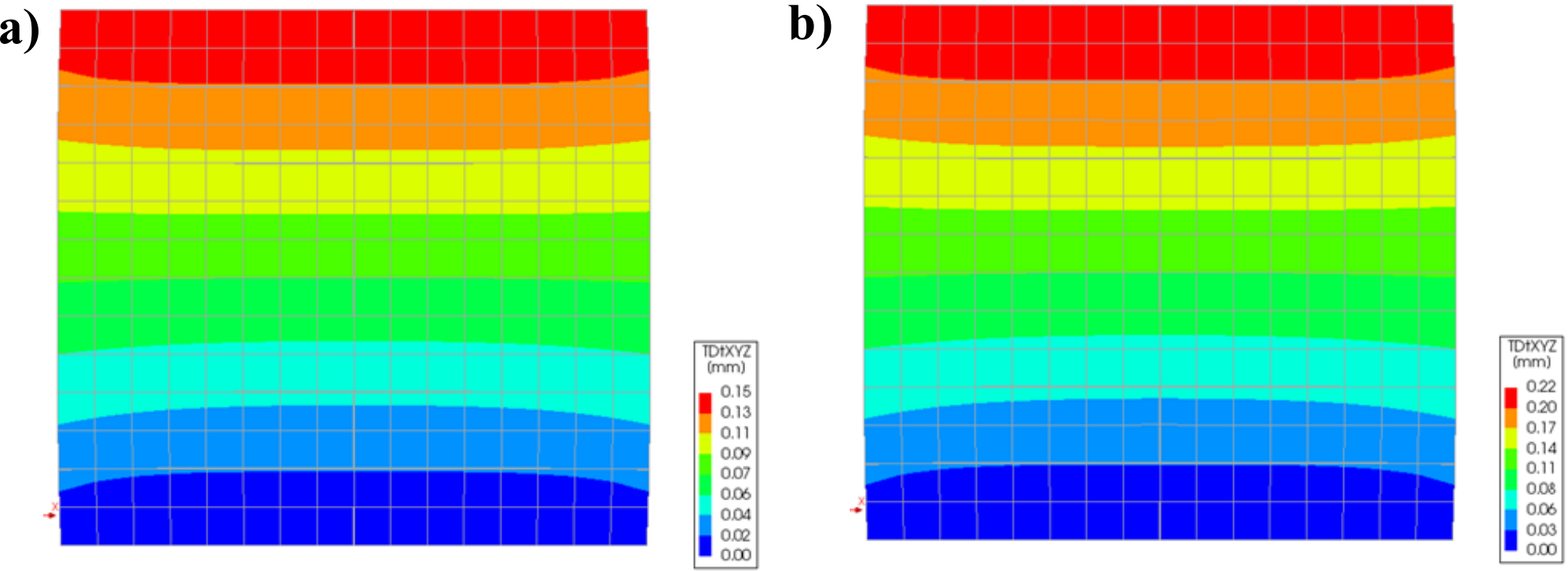
a)
TDtXYZ
(mm)
0.15
0.13
0.11
0.09
0.07
0.06
0.04
0.02
0.00
b)
TDtXYZ
(mm)
0.22
0.20
0.17
0.14
0.11
0.08
0.06
0.03
0.00

Table 1 Average mechanical properties obtained from tests on small samples.

Material	f_c [N/mm^2]	E [N/mm^2]	f_{flex} [N/mm^2]
Brick	9.62 (0.227)	2570 (0.297)	3.65 (0.066)
Mortar	3.00 (0.217)	920 (0.382)	0.92 (0.250)
Couplets	6.01 (0.035)	2025 (0.332)	-

Note: coefficient of variation indicated in parentheses

Table 2 Mechanical properties obtained from compression tests on masonry panels.

Panel	f_c [N/mm^2]	E [N/mm^2]	G_c [N/mm]	ν [N/mm^2]
V1	1.85	1776	22.13	0.18
V2	2.77	1453	4.47	0.14
Average vertical	*2.31*	*1615*	*13.30*	*0.16*
H1	2.63	3999	23.19	0.20
H2	2.59	2425	24.59	-
Average horizontal	*2.61*	*3212*	*23.89*	*0.20*
Average	***2.46***	***2610***	***18.60***	***0.17***

Table 3 Comparison of present experimental findings with data from the literature.

Reference	f_{cu} $[N/mm^2]$	f_{cm} $[N/mm^2]$	f_{cwv} $[N/mm^2]$	f_{cwh} $[N/mm^2]$	f_{cc} $[N/mm^2]$	c/b $[-]$
Present study	9.62	3.00	2.31	2.61	6.01	0.33
(Segura et al., 2018)	17.93	1.91	6.51	-	-	
(Drougkas, Verstrynge, et al., 2019)	9.97	1.70	4.70	-	8.12	0.61
(Verstrynge et al., 2011)	15.30	0.94	2.54	-	8.02	0.00
(Drougkas, Roca, et al., 2019)	35.00	8.34	15.20	16.90	20.20	1.00
(Page, 1983)	15.41	5.08	8.01	8.69	-	

Table 4 Material parameters for the numerical model of the masonry panels

Material	Parameter	Symbol	Value	Units
Brick Units	Density	ρ_b	1875[a]	Kg/m^3
	Poisson's ratio	ν_b	0.2[c, b]	
	Young's modulus	E_b	2570[a]	N/mm^2
Joint Interfaces	Normal stiffness	$k_{n,i}$	119[a]	N/mm^3
	Shear stiffness	$k_{s,i}$	22 [a]	N/mm^3
	Tensile strength	$f_{t,i}$	0.2[c]	N/mm^2
	Tensile fracture energy (Mode I)	$G_{t,i}$	0.012[c]	N/mm
	Cohesion	c_i	1.2 $f_{t,i}$ [c]	N/mm^2
	Friction angle	φ_i	36.9[c]	-
	Dilatancy angle	ψ_i	0	-
	Shear fracture energy (Mode II)	$G_{s,i}$	0.125[c]	N/mm
	Compressive strength	$f_{c,i}$	2.31[a]	N/mm^2
	Compressive fracture energy	$G_{c,i}$	5.56[a], 13.30[b], 18.6[b]	N/mm

Note: [a] : from tests on small samples, [b] : from tests on panels, [c] : from literature

Table 5 Numerical analysis results from the masonry panel models.

Parameter	Symbol	Vertical	Horizontal	Units
Young's Modulus	E_m	1856	2291	N/mm^2
Poisson's ratio	ν_m	0.15	0.20	-
Compressive strength	$f_{c,m}$	2.31	2.60	N/mm^2

Table 6 Poisson's ratio of wallettes derived from DIC data.

	Poisson's ratio	
Sample	Inner	Outer
V1	0.198	0.161
V2	0.137	0.174
Average vertical	0.168	0.168
H1	0.216	0.277
H2	0.223	0.785
Average horizontal	0.220	0.531